Sensors & Actuators: B. Chemical 429 (2025) 137258

Contents lists available at ScienceDirect

Sensors and Actuators: B. Chemical

journal homepage: www.elsevier.com/locate/snb

Open-layered MBenes: Comparisons of different wet etching techniques and electrochemical detection of heavy metal ions with high sensitivity & selectivity

Shudan Wei, Girish Kale *, Xiaojun Lai *

School of Chemical and Process Engineering, University of Leeds, Leeds LS2 9JT, United Kingdom

ARTICLE INFO

Keywords:
MBenes
Wet Etching
Open-layered
Electrochemical detection
Heavy metal ions
Density Functional Theory (DFT)

ABSTRACT

Despite significant progress in MBenes preparation and application in electrochemistry, achieving perfect layered structures and high purity under different etching conditions remains challenging. Additionally, their potential for electrochemical detection of heavy metal ions is underexplored. This study compares non-fluoride etchants for synthesizing MBene MoB from MoAlB and explores new applications in heavy metal ions detection. Ammonium persulfate (APS) etchant achieves a high Al etching rate of ~71 %, resulting in restacked accordion-like MBene, but high temperatures lead to stable, insoluble Al_xO. $CuCl_2$ has a lower etching rate of ~54 %, producing flake structures with copper impurities. Acid etching yields a perfect layered structure but a lower etching rate, while alkali etching provides similar rate to APS with the highest purity. Complete Al removal at higher temperatures causes loss of the layered structure. Our research demonstrates that some maintaining Al during hydrothermal etching maintains the layered structure, with subsequent room-temperature etching producing fluffy open-layered MoB (OL-MBene). Electrochemical studies showed OL-MBene-modified GCE performs excellently in detecting Cd^{2+}, Pb^{2+}, Cu^{2+}, and Hg^{2+}, with high sensitivity and selectivity, especially for Cu^{2+} and Pb^{2+}. Pb^{2+} shows the highest sensitivity due to its lowest adsorption energy on the MBene surface. Competitive adsorption studies indicate Pb^{2+} competes with Hg^{2+} for adsorption sites but minimally impacts Cd^{2+} and Cu^{2+} adsorption. This research enhances understanding of MBene synthesis and introduces a new method for sensitive electrochemical sensors.

1. Introduction

2D transition metal borides, commonly referred to as MBenes, have emerged as a significant class of materials within the realm of nanotechnology due to their unique and remarkable properties [1]. These materials, derived from the etching of layered ternary borides, possess a range of attributes that make them highly suitable for applications in areas such as catalysis [2], energy storage [3], and gas sensing [4]. The previous findings and exciting observations on 2D transition metal carbides/nitrides (MXenes) in ions/small molecules sensing [5,6] have motivated us to thoroughly investigate the ion detection behavior of functionalized MBenes. MBenes, with their outstanding physicochemical, electronic, and mechanical properties, provide an ideal platform for absorbing small ions and molecules, making them highly promising for catalysis and sensing applications [7–9]. Although MBenes have great potential for the electrochemical detection of heavy metal ions-a critical capability for environmental monitoring and public health. There has been no experimental and theoretical research on this topic until now.

Traditional synthesis methods for MBenes typically involve processes such as chemical etching [1,8,10,11] or high-temperature (500–800 ℃) solid-state Lewis base reduction etching of Aluminum from the parent MAX phases [12,13]. These methods usually yield materials with an accordion-like structure, where layers tend to restack due to high surface energy. This restack significantly reduces the exposure of active surfaces, thereby diminishing the electrochemical performance of the materials. Consequently, there is a pressing need for innovative synthesis techniques that can prevent restacking and maintain the structural integrity and functionality of MBenes. The chemical wet etching process is more economical, milder, and yields higher purity products, but the traditional etchant is Fluoride, dangerous, and environmentally unfriendly. Recent studies found that alkali and acid could realize some Al etching [3], which are much milder. In the specific case of MoAlB wet

* Corresponding authors.
E-mail addresses: G.M.Kale@leeds.ac.uk (G. Kale), X.Lai@leeds.ac.uk (X. Lai).

https://doi.org/10.1016/j.snb.2025.137258
Received 16 September 2024; Received in revised form 25 December 2024; Accepted 11 January 2025
Available online 15 January 2025

etching, the relatively low chemical state of Al facilitates its removal through reactions with various bases, acids, Lewis bases, or oxidizers. Here, we first used and compared these 4 kinds of etchant for MoAlB etching, and subsequent room temperature etching for producing fluffy open-layered MBene phase MoB (OL-MBene).

Heavy metal ions such as Cadmium (Cd), lead (Pb), copper (Cu), and mercury (Hg) are known for their toxicity and persistence in the environment [14]. These contaminants can accumulate in living organisms, leading to severe health issues including neurological damage, kidney failure, and various cancers [15–17]. The presence of heavy metals in water, soil, and food sources is a major concern worldwide, necessitating the development of efficient and reliable detection methods [18,19]. A metal ion detector is a device or instrument used to detect the presence of metal ions in its surrounding environment, and sometimes it can also be used to quantify these metal ions [20]. There are three typical techniques for heavy metal ion detection: Spectroscopic detection, Electrochemical methods of detection, and Optical methods of detection [20]. Conventional techniques spectroscopic detection for heavy metal ions detection, such as atomic absorption spectroscopy (AAS) [20] and inductively coupled plasma mass spectrometry (ICP-MS) [21], offer high sensitivity and accuracy but are often expensive, time-consuming, and require sophisticated instruments requiring skilled personnel [22]. Optical detection is relatively simple and easy to perform, but some methods may have lower sensitivity and unstable reagents [23]. Electrochemical methods detect metal ions based on their unique signature redox properties [24]. These methods measure the current, voltage, or impedance changes resulting from the electrochemical reactions of metal ions at an electrode surface [25] with high sensitivity and selectivity, portable and relatively low-cost equipment, fast response time and the ability to perform real-time monitoring [26,27]. But some existing electrodes are very expensive and interference from other ions or substances in the sample can affect accuracy. Therefore, there is an urgent need for portable, cost-effective, and highly sensitive methods for on-site detection of heavy metal ions.

This study presents a pioneer investigation into the application of MBenes for electrochemical sensing of heavy metal ions. We systematically explored the etching behaviors of MoAlB using various non-fluoride etchants, elucidating their effects on the structural morphology and material purity of MBene MoB. Additionally, we evaluate the electrochemical properties of the resulting open-layered MBene (OL-MBene), specifically its effectiveness in detecting Cd^{2+}, Pb^{2+}, Cu^{2+}, and Hg^{2+}. Moreover, to gain a deeper understanding of the adsorption mechanisms at play, we employ density functional theory (DFT) simulations. These simulations provide insight into the interaction energies and affinities between the OL-MBene surface and different metal ions, elucidating the underlying principles that govern the material's superior performance. This research advances our understanding of MBene synthesis and characterization, introducing a new avenue for highly sensitive and selective electrochemical sensors for environmental monitoring. The potential of MBenes extends to advanced technological domains, paving the way for high-performance electrodes in catalysis, energy storage systems, and beyond.

2. Experimental section

2.1. Preparation of MBenes

200 mg of 500 mesh MoAlB was introduced into 50 mL of 0.25 M ammonium persulfate APS, $CuCl_2$, NaOH, and H_2SO_4 solutions within a sealed 200 mL autoclave. The autoclave was subsequently placed in an electric thermostatic drying oven, and the temperature was carefully controlled at 180 ℃ for 6 hours. The obtained materials were then thoroughly rinsed with deionized water until reaching a pH of approximately 7, followed by separation from the solution through centrifugation at 8000 rpm. Subsequently, the materials were dried overnight at 60 °C. To obtain a fluffy open-layered MBene the above NaOH etching product was subjected to stirring in 0.25 M NaOH/ 5 M ammonium hydroxide solution for 24 hours at RT, yielding a product called OL-MBene. We also introduced the interlayer agent Tetramethylammonium hydroxide (TMAOH) for intercalation.

2.2. Characterization

The prepared sample underwent comprehensive analysis to reveal its elemental composition, morphology, and structure. A scanning electron microscope (SEM, Hitachi TM3030) with energy-dispersive X-ray analysis (EDX) was employed to scrutinize the sample's surface. The confirmation of the sample's formation and insights into its crystallinity were derived from X-ray diffraction (XRD, Bruker D8). To evaluate the electrochemical properties, AUTOALB PGSTAT101 potentiostat/galvanostat was utilized.

2.3. Electrode preparation and electrochemical measurement

5 mg of OL-MBene was dispersed in 500 μL of isopropanol and then mixed with 25 μL of 5 wt% Nafion solution under sonication for 2 h to form a homogeneous solution. After that, 4 μL of the ink was drop-casted on an L-type glassy carbon electrode (GCE) with a 3 mm diameter to form a uniform electrode film, and the solvent was volatilized at room temperature to obtain the sensing electrode OL-MBene@GCE. The electrochemical cell was assembled with a conventional three-electrode system: a modified glassy carbon electrode as the working electrode, a Pt mesh as the counter electrode and an Ag/AgCl in saturated KCl solution as the reference electrode, against which all electrochemical measurements were conducted in this study. Since all the electrochemical measurements were conducted in pH 4 electrolyte, the electrode was activated in pH 4 H_2SO_4 solution under 20 mV s^{-1} cyclic voltammetry scanning (-1–1 V) for 20 cycles. Electrochemical impedance spectroscopy (EIS) measurements were conducted in the frequency range from 100 kHz to 0.1 Hz at 10 mV modulation amplitude.

Square wave anodic stripping voltammetry (SWASV) measurements were performed for the detection of heavy metal ions in buffer solution (pH 4.0) containing Cd^{2+}, Pb^{2+}, $Cu^{2+}$and Hg^{2+}. The preconcentration step was carried out at the potential of −1.0 V for 100 s with stirring. After an equilibration period of 15 s, the anodic stripping voltammograms were recorded in the potential range from −1.0–0.5 V. The square-wave potential scan was applied with an incremental potential of 4 mV, amplitude of 25 mV and frequency of 15 Hz. A desorption potential of 1 V was used for 200 s to remove the residual heavy metal ions under constant stirring conditions after each anodic stripping measurement. All the experiments were carried out at room temperature in an ambient solution.

2.4. Computational method

Geometry optimization, energy calculations and properties simulation were calculated using the Cambridge Serial Total Energy Package (CASTEP). The GGA-PBE functional was utilized to address the exchange-correlation potential [28]. The cutoff energy of the plane wave basis is set to 500 eV, the special *k*-points sampling integration over the Brillouin zone was employed using the Monkhorst Pack method the pseudopotentials chosen are OTFG ultrasoft pseudopotentials. The Broyden-Fletcher-Goldfarb-Shanno (BFGS) algorithm was selected with convergence criteria set to 5.0×10^{-6} eV/atom for energy and 0.01 eV/Å for force [29]. Additionally, when optimizing geometry and calculating the absorption energy of heavy metal ions (M^{2+}), to prevent interactions between layers, a vacuum layer of 20 Å was introduced in the *z*-axis direction of the 2D structure and a $3 \times 3 \times 1$ k-point grid was employed for supercell MoB [30]. The adsorption energy of heavy metal ion M^{2+} on the MoB surface was calculated using Eq. 1:

$$E_{ads.} = E_{(MBene-M)} - E_M - E_{MBene} \quad (1)$$

$E_{ads.}$ is the adsorption energy, $E_{(MBene-M)}$, $E_{M,\ and}$ E_{MBene} are the total energy of heavy metal ion M^{2+} adsorbed on MBene, the energy of only M^{2+} and MBene, respectively.

3. Results and discussion

3.1. Preparation and characterization

In the specific case of MoAlB wet etching, the relatively low chemical state of Al facilitates its removal through reactions with various bases, acids, Lewis bases, or oxidizers. Here we compare the etching effects of various non-fluoride etchants. Using Ammonium persulfate (APS), we achieved a substantial etching rate of approximately 71 % for Al, resulting in an accordion-like multilayered but restacked MBene material (Fig. 1a, Table S1). However, due to significant oxidation, stable and insoluble Aluminum oxides formed under hydrothermal high temperatures, reducing product purity. Energy-dispersive X-ray spectroscopy (EDS) analysis (Fig. S1) revealed that black by-products primarily consisted of insoluble Aluminum compounds that resisted dissolution even in HCl. When using the Lewis base $CuCl_2$, an etching rate of approximately 54 % was achieved, yielding products with flake and plate structures (Fig. 1b) that lacked the desired layered morphology and contained considerable copper impurities (Fig. S2). Acid etching resulted in an etching rate of about 33 %, but the structure was perfectly layered, and the products were pure (Fig. 1c). Alkali etching achieved etching rates similar to those of APS but with the highest product purity. Simple water washing was sufficient to remove the etchant, leaving a high-purity accordion-like MBene (Fig. 1d). The chemistry of etching relations with the four etchants is as follows:

$$(NH_4)_2S_2O_8 + MoAlB + H_2O \rightarrow (NH_4)_2SO_4 + Al_xO + MoB \quad (2)$$

$$CuCl_2 + MoAlB \rightarrow AlCl_3 + Cu + MoB \quad (3)$$

$$MoAlB + H^+ \rightarrow MoB + Al^{3+} + H_2 \quad (4)$$

$$MoAlB + H_2O + OH^- \rightarrow MoB + H_2 + AlO_2^- \quad (5)$$

X-ray diffraction (XRD) analysis following alkali etching showed the complete loss and transformation of the MoAlB phase (MoAlB > pdf 65–2497) [8] after etching in 0.25 M NaOH at 180°C (Fig. 1e), indicating thorough etching [3]. In contrast, under acidic conditions where the Al removal rate is only ~33 %, the crystal phase remains as the precursor MoAlB. When the removal rate exceeds 50 %, as with $CuCl_2$, all phases transform to Mo_2AlB_2 and MoB [3]. However, etching with $CuCl_2$ and APS results in some impurities, leading to unexpected peaks (marked in black diamonds, Al_xO in APS, and Cu in $CuCl_2$). Furthermore, at elevated etching temperatures up to 220°C, complete Al removal was achieved, resulting in the loss of the layered structure (Fig. 1f), and precursor MoAlB in Fig. 1g for comparisons. This observation suggests that the high surface energy of the layered material promotes restacking at high temperatures, leading to the loss of the layered structure. It is hypothesized that retaining a small amount of Al during hydrothermal etching helps support and maintain the layered structure. This approach is also widely recognized in the synthesis of two-dimensional transition metal carbides, known as MXenes. Guo et al. [31] found that partially retaining Al during the etching of Ti_3AlC_2 results in a more open-layered structure, while the reserved Al ensures good conductivity.

After hydrothermal alkaline etching at 180°C, the material was cooled to room temperature and stirred in dilute NaOH for an additional 24 hours. This process led to the further removal of a small amount of Al (~5 %), resulting in a fluffier open-layered structure, referred to as OL-MBene (Fig. 2a-b). This result was consistent even when using weaker base ammonia as the etchant at room temperature (Fig. 2c). However, the commonly used intercalating agent TMAOH (tetramethylammonium hydroxide) did not achieve this effect (Fig. 2d). The structures and etching rates obtained with all etchants are summarized in Table S1. Therefore, we conclude that while removing Al is crucial for forming more layers, retaining a small amount of Al is necessary to maintain stable layered structures.

3.2. Electrochemical properties

Graphene is widely used in electrochemical sensors. However, many of its composites are typically limited to detecting one or two metal ions [32]. Recently, MXenes have also been explored for metal ion sensing, but their easily oxidized surface affects their stability [33]. MBene shares key properties with graphene, such as a multilayered structure and high conductivity, while offering greater interfacial stability and unique features [3]. Elements in MBene, such as molybdenum (Mo), titanium (Ti), and vanadium (V), have a high affinity for heavy metal ions, making MBene particularly suited for ions detection. This study is the first to demonstrate MBene's potential as an effective material for

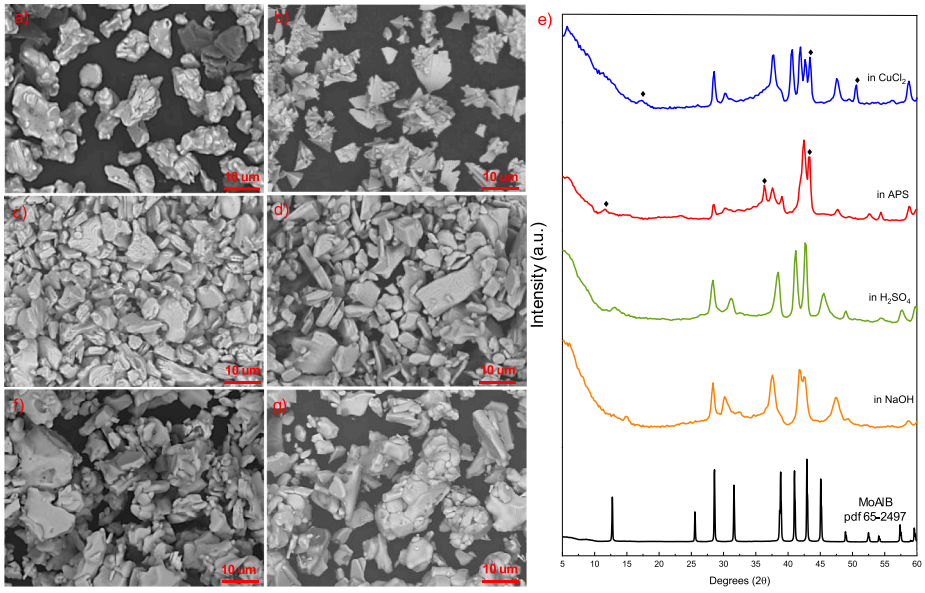

Fig. 1. SEM photographs of MoAlB etched at 180 ℃ for 6 h in 0.25 M a) APS, b) $CuCl_2$, c) H_2SO_4, d) NaOH, e) XRD patterns of MoAlB and its etching product in different 0.25 M etchants at 180 ℃, f) SEM photographs of MoAlB etched at 220 ℃ for 6 h in 0.25 M NaOH, g) SEM of precursor MoAlB.

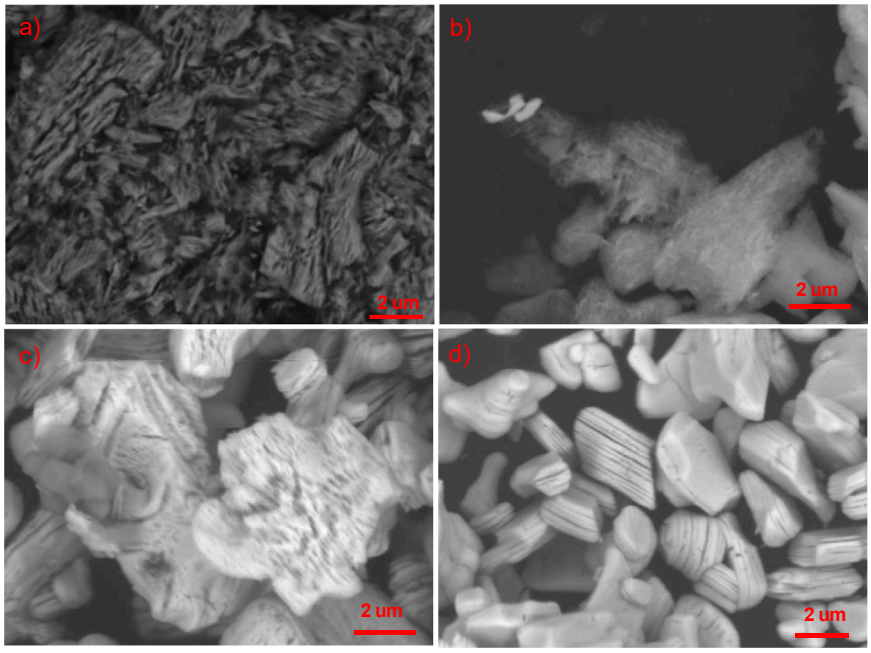

Fig. 2. SEM photographs of MoAlB etched at 180℃ and then stirred at RT for 24 h in a) and b) 0.25 M NaOH, c) 5 M NH_4OH, and d) TMAOH (25 wt% in water).

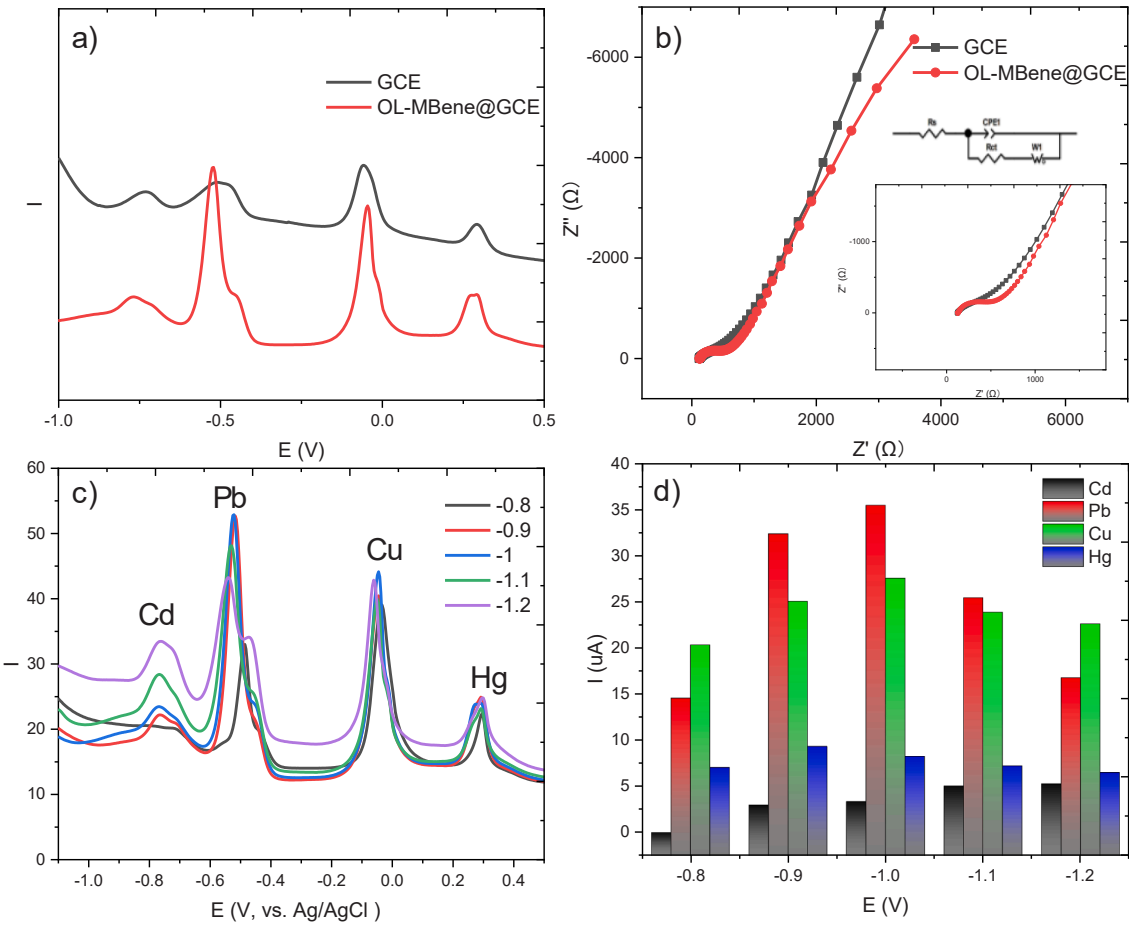

Fig. 3. a) Comparison of SWASV curves on GCE and OL-MBene@GCE electrodes for the simultaneous detection of 1 μM Cd^{2+}, 1 μM Pb^{2+}, 1 μM Cu^{2+}, and 2 μM Hg^{2+} at a deposition potential of −1 V, b) Nyquist plots obtained by electrochemical impedance spectroscopy (EIS), with enlargement and equivalent series resistance (ESR) in the insets, c) SWASV curves on OL-MBene@GCE at deposition potentials ranging from −0.8 V to −1.2 V, d) response current of different ions at various deposition potentials.

the electrochemical sensing of heavy metal ions.

The electrochemical characterization of OL-MBene@GCE was evaluated using SWASV for the simultaneous detection of 1 μM Cd^{2+}, 1 μM Pb^{2+}, 1 μM Cu^{2+}, and 2 μM Hg^{2+} in a mixed pH 4 solution, compared to bare GCE. As shown in Fig. 3a and Table S2, four well-defined stripping peaks were observed on the MBene-modified electrodes, demonstrating higher peak currents than those observed with bare GCE. EIS was also employed to characterize the interface properties of the modified electrodes (Fig. 3b, Table S3). The solution resistances were almost identical after modifying OL-MBene, indicating that MBene possesses good conductivity. The semicircular portion observed at higher frequencies corresponds to the electron transfer-limited process (R_{ct}). The R_{ct} value for OL-MBene@GCE is 382.9 Ω, larger than that for bare GCE, which is attributable to the layered structure requiring some time for diffusion. However, this value is similar to that of MXene and is acceptable[33]. To ensure the complete dissolution of metal ions, the used detection pH is 4. Deposition potential is a critical factor for the electrochemical detection of heavy metal ions. As shown in Figs. 3c, 3d and Table S4, deposition potentials ranging from −1.2 to −0.8 V showed that the stripping currents of all four metal ions were comparatively higher at more negative potentials. However, as the deposition potential became more negative, especially in −1.2 V, reproducibility decreased due to more significant hydrogen evolution in the acetate buffer. Thus, −1 V was chosen for all subsequent experiments to achieve high sensitivity and reproducibility.

Sensitivity, selectivity, reproducibility, and linearity are critical parameters for the development of next-generation on-site electrochemical heavy metal ions sensors. The OL-MBene modified glassy carbon electrode (GCE) was employed for detecting individual heavy metal ions and co-existing Cd^{2+}, Pb^{2+}, Cu^{2+}, and Hg^{2+}. The stripping behavior of Cd^{2+} in the range of 0.5–1.9 μM and the corresponding calibration plots are shown in Fig. 4a. The linear fitting slope is 2.799 ± 0.13395 μA μM^{-1} and 39.6 μA μM^{-1} cm^{-2}, with a correlation coefficient of 0.986. The limit of detection (LOD) was calculated to be 0.112 μM using the 3σ method, where the 3σ LOD is calculated from 3 SD/S (SD is the standard deviation of the measurements, and S is the slope of the calibration plot). The stripping behaviors of Pb^{2+} and Cu^{2+} were also examined in the ranges of 0.1–0.9 μM and 0.5–1.2 μM, respectively (Fig. 4b and c), demonstrating much higher sensitivity compared to Cd^{2+}. The calibration curve slopes were 31.152 ± 0.79579 μA μM^{-1} (440.923 μA μM^{-1} cm^{-2}) and 27.06 ± 0.40473 μA μM^{-1} (383.01 μA μM^{-1} cm^{-2}) for Pb and Cu ions, respectively. The LODs were 0.0481 μM for Pb^{2+} and 0.0495 μM for Cu^{2+}. For Hg^{2+}, the linear fitting slope was 12.227 ± 0.41048 μA μM^{-1}, with a correlation coefficient of 0.994 and an LOD of 0.0678 μM. These results also summarized in Table 1 indicate that the OL-MBene modified GCE is capable of detecting Cd^{2+}, Pb^{2+}, Cu^{2+}, and Hg^{2+} individually, with excellent electrochemical performance, particularly towards Cu^{2+} and Pb^{2+}.

The deposition time, linear range, sensitivity, and detection limit for Cd^{2+}, Pb^{2+}, Cu^{2+}, and Hg^{2+} were compared with previously reported values using various electrode materials (Table S5). Our results show that the sensitivity of the OL-MBene-modified GCE is at a medium to high level compared to commonly used materials, particularly demonstrating high sensitivity for the detection of lead and copper. The limits of detection (LOD) obtained in our work are comparable to those reported in other studies. These results are expected to pave the way for a series of promising electrode materials based on the MBene family.

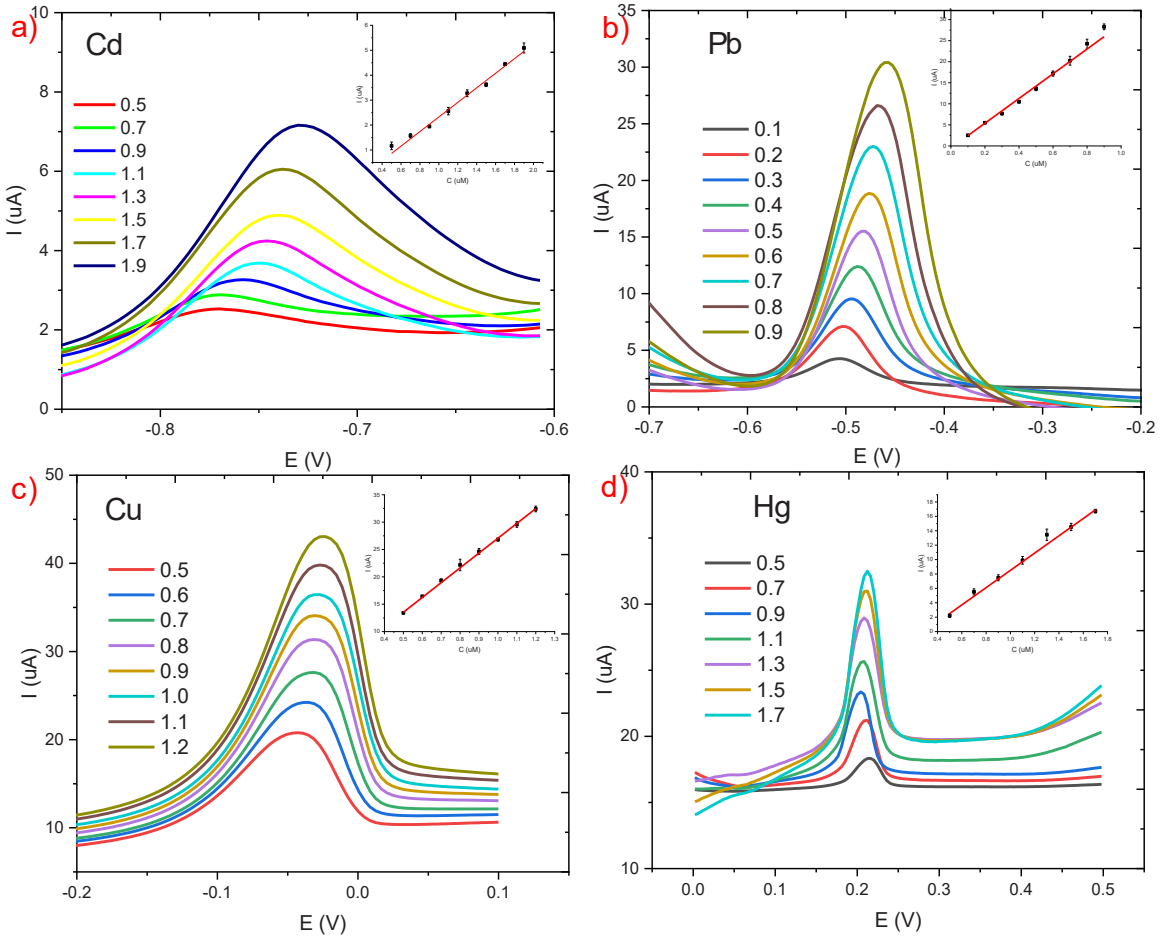

Fig. 4. SWASV response of the OL-MBene@GCE for individual analysis of (a) Cd^{2+}, (b) Pb^{2+}, (c) Cu^{2+}, and (d) Hg^{2+}. Insets display the corresponding linear calibration plots of peak current against Cd^{2+}, Pb^{2+}, Cu^{2+}, and Hg^{2+} concentrations, respectively.

Table 1
Fitting results of OL-MBene for individual sensing Cd^{2+} Pb^{2+}, Cu^{2+} and Hg^{2+}. Data in column-4 correspond to the values in column-3 normalised with respect to the electrode surface area.

Ions	Linear range (μM)	Sensitivity (μA $μM^{-1}$)	Sensitivity (μA $μM^{-1}$ cm^{-2})	Correlation coefficient	LOD (μM)
Cd^{2+}	0.5–1.9	2.799 ± 0.13395	39.6	0.986	0.112
Pb^{2+}	0.1–0.9	31.152 ± 0.79579	440.923	0.995	0.0481
Cu^{2+}	0.5–1.2	27.06 ± 0.40473	383.01	0.997	0.0495
Hg^{2+}	0.5–1.7	12.227 ± 0.41048	173.06	0.994	0.0678

Multiple co-existing metal ions are frequently encountered in practical sensing applications. Mutual interference among these components poses a significant challenge for detecting and calibrating the target contamination with high precision and sensitivity. The simultaneous Cd^{2+}, Pb^{2+}, Cu^{2+}, and Hg^{2+} determination was performed in a mixed solution using the OL-MBene modified GCE (Fig. 5a, b). The corresponding linearization slopes were 2.48, 30.74, 25.7, and 2.93 μA $μM^{-1}$ for Cd^{2+}, Pb^{2+}, Cu^{2+}, and Hg^{2+}, respectively, with correlation coefficients of 0.997, 0.999, 0.999, and 0.946 (Table S6). All four species exhibited well-separated voltametric peaks without significant mutual interference as metal ion concentrations increased, providing solid evidence that the modified GCE electrode can serve as a reliable platform for the simultaneous and selective detection of co-existing metal ions. The stripping values of Cd, Pb, and Cu did not show much difference compared to their individual result. However, Hg^{2+} exhibited a much lower responding current in a simultaneous detection system. This variation between multiple and single target detection is attributed to intermetallic interferences. In higher Pb^{2+} concentration solutions, the stripping signal of 0.5 μM Hg decreased as Pb^{2+} concentration increased, indicating that the detection of Hg^{2+} was disturbed by Pb^{2+}. In contrast, the responses of Cd^{2+} and Cu^{2+} did not change significantly with increasing Pb^{2+} concentration, suggesting they are less affected by Pb^{2+} and each other. This phenomenon is likely related to the different adsorption energies of metals on the MBene surface. We further investigated this through DFT calculations.

We studied the adsorption mechanism of a single metal (M^{2+}) ion on the MBene MoB electrode surface. Based on the symmetry of MoB, there are four possible adsorption sites for M ion adsorption on the electrode surface: S1, S2, S3, and S4, as shown in Fig. 6a and Table S7. S1 is the site on top of a B atom surrounded by four Mo atoms; S2 and S4 are different bridge sites between two Mo atoms; and S3 is on top of a Mo atom (Fig. 6a and b). The adsorption energies for these four sites are shown in Fig. 6c and Table S7. Site S1 has the most negative adsorption energy because it is located in a cavity surrounded by four Mo atoms, providing stable electron donation and resulting in the most stable adsorption. The bridge sites, S2 and S4, have similar adsorption energies, being encapsulated by two Mo atoms each. The site on top of the Mo atom (S3) has the highest adsorption energy. This preference for adsorption sites indicates that Site 1 possesses the most favorable conditions for binding,

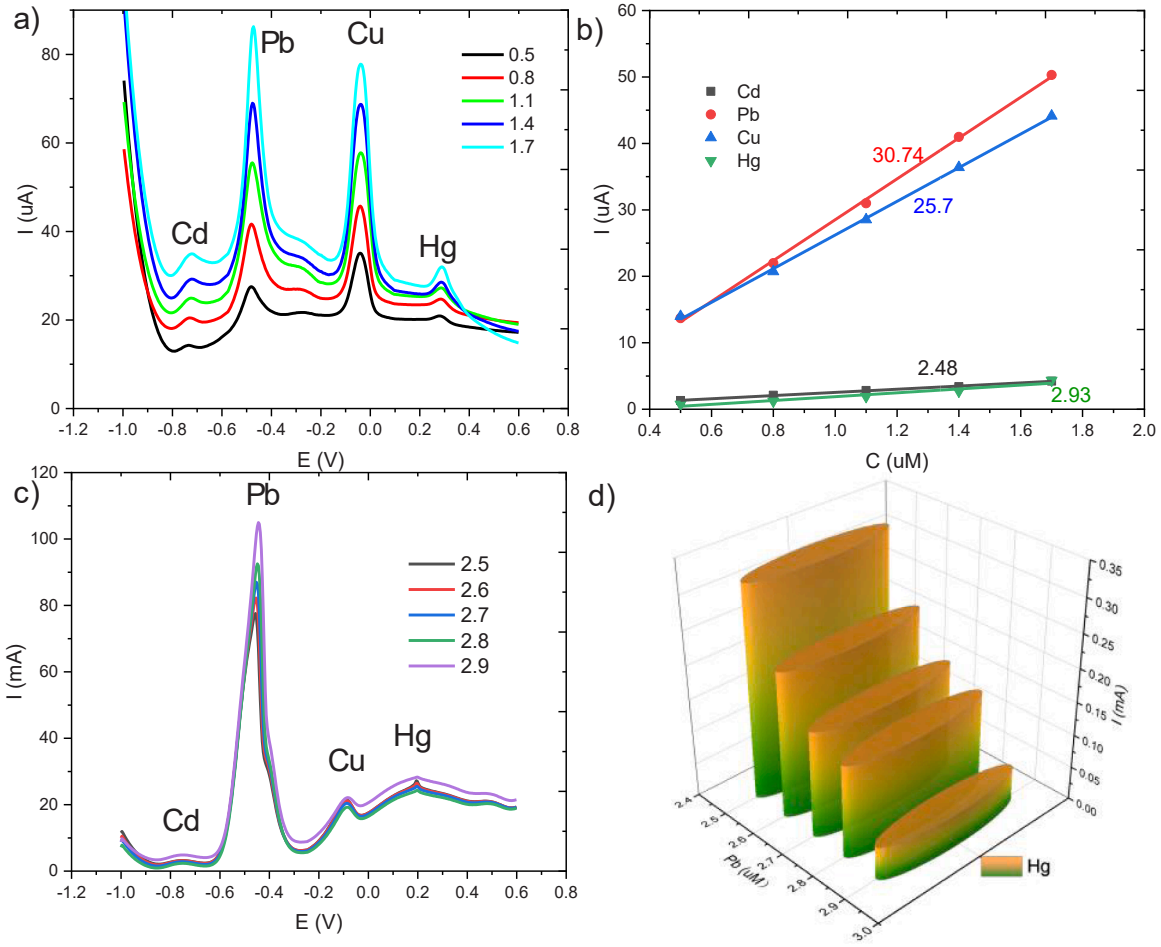

Fig. 5. (a) SWASV response of the OL-MBene@GCE for the simultaneous analysis of Cd^{2+}, Pb^{2+}, Cu^{2+}, and Hg^{2+}, (b) respective calibration curves for Cd^{2+}, Pb^{2+}, Cu^{2+}, and Hg^{2+} corresponding to panel (a), (c) SWASV response of the OL-MBene@GCE for the simultaneous analysis of 0.5 μM Cd^{2+}, Cu^{2+}, and Hg^{2+} in the presence of 2.5–2.9 μM Pb^{2+}, (d) response current of Cu^{2+} at different concentrations of Pb^{2+} related to (c).

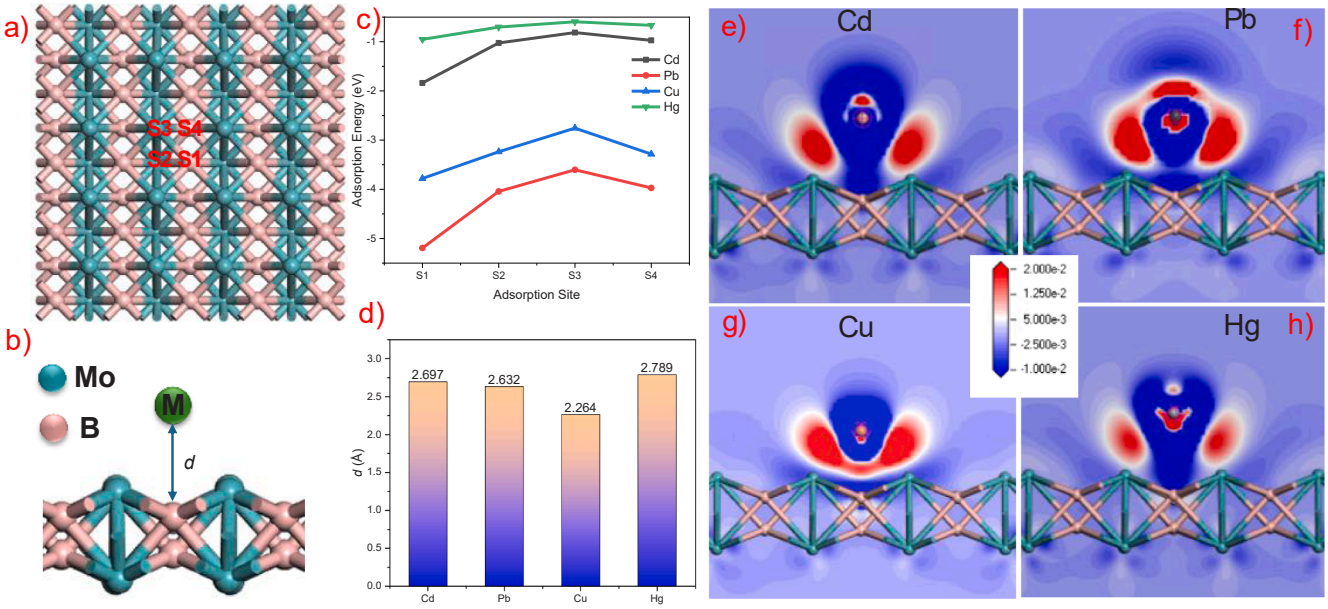

Fig. 6. a) Top view of absorption site of heavy metal ions on MBene, b) side view of site 1 absorption with distance of B-M, c) adsorption energy of M^{2+} on the surface of MBene MoB in diversity sites, d) distance of M-B in site S1, e∼h) slices of charge density difference between the adsorbed M ions (Cd^{2+}, Pb^{2+}, Cu^{2+}, Hg^{2+}) and MBene MoB.

likely due to factors such as most negative surface energy, better electronic compatibility, or optimized spatial geometry for interaction. As a result, all metal ions tend to prioritize adsorption on Site 1 before occupying less favorable sites like S2 and S4. Adsorption on Site 3 appears to be the least likely due to its less advantageous structural or electronic properties. The adsorption energy (in eV) varies across different sites for each metal ion. Overall, the trend in adsorption energies is $Pb^{2+} > Cu^{2+} > Cd^{2+} > Hg^{2+}$ (more negative adsorption energies), which explains why Pb^{2+} exhibits the highest sensitivity, followed closely by Cu^{2+}, Cd^{2+} and then Hg^{2+} with less negative adsorption energies, particularly Hg^{2+}—exhibit lower sensitivity.

This trend also highlights distinct correlations between adsorption energies, ionic size, and electronic properties. Smaller ions, such as Cu^{2+} (radius 0.73 Å, Table S7), tend to exhibit more negative adsorption energies at specific sites, indicating stronger interactions with the adsorption surface than larger ions like Cd^{2+} and Hg^{2+}. These findings emphasize the importance of both ionic size and electronic configuration in determining adsorption strength and the resulting electrochemical sensitivity of the system. Interestingly, Pb^{2+}, despite having the largest ionic radius among the studied ions, shows the strongest adsorption energy, suggesting that factors beyond ionic radius, such as electronic structure or hybridization effects, significantly influence adsorption behavior. Across all adsorption sites, the general trend suggests more negative adsorption energies as the ionic radius decreases, with Pb^{2+} being an exception likely due to atomic or electronic effects. Furthermore, as ionic radius increases ($Cu^{2+} \rightarrow Cd^{2+} \rightarrow Hg^{2+} \rightarrow Pb^{2+}$), the B-M bond height at Site 1 follows a rising trend but drops for Pb^{2+}, which is the ion with the largest radius (Figs. 6b, 6d and Fig. S3). This deviation highlights the complex interplay between ionic size and other influencing factors. For Cu^{2+}, the smaller radius corresponds to a shorter M-B bond distance, indicating closer and stronger interactions with the adsorption site. This observation supports the hypothesis that a smaller ionic radius enhances binding strength through stronger electrostatic or covalent interactions with the substrate. However, the deviation observed for Pb^{2+} implies that electronic effects, such as charge density, polarization, or specific orbital interactions, may play a crucial role. Further investigations into these electronic properties would provide a more comprehensive understanding of the observed trends and deviations.

Charge density difference slices between M and MBene are shown in Fig. 6e-h to elucidate the underlying mechanism. Here, $\Delta\rho = \rho_{MBene\text{-}M} - \rho_{MBene} - \rho_M$, where $\rho_{MBene\text{-}M}$, ρ_{MBene}, and ρ_M are the electron densities of MBene MoB with adsorbed metal ions, the bare MBene electrode, and a single metal ion, respectively. Significant electron depletion was observed around the heavy metal ions, indicating electron transfer from M to the electrode MBene. The transferred electrons primarily accumulated around Mo atoms on MBene, with the most accumulation occurring for Cu and Pb, followed by Cd, and the least for Hg. This electron transfer contributes to stronger adsorption and higher selectivity and sensitivity. Based on the analysis of the above experimental results and simulation analysis, lead competes with mercury for adsorption sites, while it has minimal impact on the adsorption of copper and cadmium.

The stability of the OL-MBene@GCE was evaluated by performing nine consecutive measurements of mixed 1 μM Cd^{2+}, 1 μM Pb^{2+}, 1 μM Cu^{2+}, and 1 μM Hg^{2+} solution under optimized experimental conditions. The SWASV responses for the four target heavy metal ions exhibited excellent reproducibility, with a high degree of overlap among the SWASV curves (Fig. 7a). The relative standard deviation (RSD) values were determined to be 7.43 % for Cd^{2+}, 0.81 % for Pb^{2+}, 1.21 % for Cu^{2+}, and 5.32 % for Hg^{2+}, respectively. As shown in Fig. 7b, reproducibility was further assessed through the simultaneous detection of the above mixed Cd^{2+}, Pb^{2+}, Cu^{2+}, and Hg^{2+} solution using four OL-MBene-modified GCEs fabricated under identical conditions. The corresponding RSD values were 8.76 % for Cd^{2+}, 0.97 % for Pb^{2+}, 1.71 % for Cu^{2+}, and 5.89 % for Hg^{2+}. These results highlight the good reproducibility of the developed electrochemical sensor, particularly for Cu^{2+} and Pb^{2+}.

An essential characteristic of a sensor is its ability to differentiate target metal ions from interfering agents present in the same environment. To evaluate this property, the SWASV peak current signals of metal ions were examined in the presence of interfering agents, using analyte solutions containing 1 μM of selected metal ion (Cd^{2+}, Pb^{2+}, Cu^{2+}, and Hg^{2+}, respectively) under the same experimental conditions as described above. The interfering agents were introduced at 10 times the concentration of the target ions, including metal cations (Zn^{2+}, K^+, Mg^{2+}, Na^+, Ca^{2+}, and Co^{2+}), anions (SO_4^{2-}, Cl^-, NO_3^-), and organic compounds (acetone, alcohol, hexane, etc.), as shown in Fig. 7c–f. The SWASV curves of the selected metal ions showed minimal deviation in the

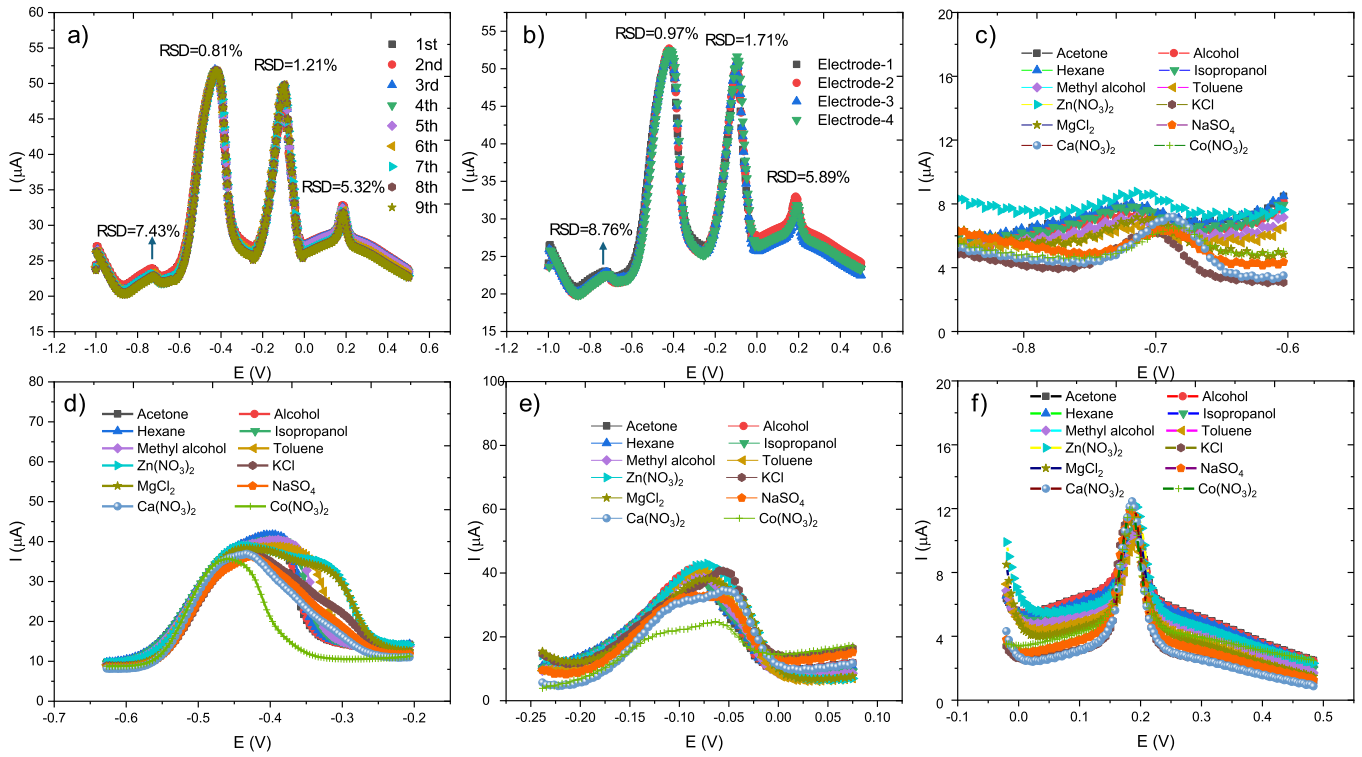

Fig. 7. SWASV curves of 1 μM Cd^{2+}, 1 μM Pb^{2+}, 1 μM Cu^{2+} and 1 μM Hg^{2+} a) under 9 repetitive detection measurements with OL-MBene@GCE, b) with 4 OL-MBene modified GCEs, SWASV obtained with OL-MBene@GCE in a solution of c)1 μM Cd^{2+}, d)1 μM Pb^{2+}, c)1 μM Cu^{2+}, d)1 μM Hg^{2} along with 10 μM of one of the following potential interfering agents: acetone, alcohol, hexane, isopropanol, methyl alcohol, toluene, $Zn(NO_3)_2$, KCl, $MgCl_2$, Na_2SO_4, $Ca(NO_3)_2$, and $Co(NO_3)_2$, respectively.

presence of organic agents, except for toluene. This slight deviation could be attributed to the chelation effect of the benzene ring in toluene [34], which may reduce the concentration of free heavy metal ions in the solution; however, the impact was relatively minor. For Cd^{2+}, the addition of Zn^{2+} caused a reduction in the response current, likely due to the similar redox potentials of Zn^{2+} and Cd^{2+}, leading to significant competitive effects [35], especially given that Zn^{2+} was present at 10 times the concentration of Cd^{2+}. In the case of Pb^{2+}, the interfering agents had negligible effects, possibly due to its high affinity for the electrode surface. For Cu^{2+}, Mg^{2+} and Co^{2+} caused slight interference, with Co^{2+} having a more pronounced impact. This suggests that in applications involving high concentrations of Co^{2+}, the sensor may not be the optimal choice for detecting Cu^{2+}. However, given that the interfering ions were present at 10 times the target ion concentrations, the interference under less concentration of Co^{2+} is expected to be less significant. Notably, Hg^{2+} demonstrated robust performance in the interference studies, maintaining stable responses across all conditions tested, further highlighting the reliability of the sensor in detecting this ion. Anions such as Cl^-, SO_4^{2-}, and NO_3^- exhibited very little impact on the target ions, as the response currents of the target ions showed minimal variation even in the presence of interfering agents containing these anions (such as KCl, Na_2SO_4 and $Ca(NO_3)_2$).

The OL-MBene@GCE was utilized to measure selected heavy metal ions in real water samples, demonstrating the feasibility of the proposed method for practical applications. For this purpose, known concentrations of metal salts were spiked into real water samples collected from various sources, including distilled drinking, and tap water (Table 2). The recoveries of the selected metal ions were determined by comparing their peak current values with the background-subtracted calibration curves. The percentage recoveries for Cd^{2+} ranged from 89 % to 90 %, while those for Cu^{2+} and Pb^{2+} exceeded 95 %, and for Hg^{2+}, ranged from 94 % to 97 %. These results highlight the precision and practicality of the surfactant-based sensor for detecting multiple toxic heavy metal ions in real water samples, with particularly high performance observed for Cu^{2+} and Pb^{2+}.

Table 2
Results for Cd^{2+}, Pb^{2+}, Cu^{2+}, and Hg^{2+} determination in real water samples.

Metal ions	Samples	Initially found (μM)	Spiked amount (μM))	Found (μM))	Recovery (%)
Cd^{2+}	Tap water	0	1	0.89	89.0 %
	Distilled water	0	1	0.9	90.0 %
Pb^{2+}	Tap water	0	1	0.985	98.5 %
	Distilled water	0	1	0.9673	96.7 %
Cu^{2+}	Tap water	0.091	1	1.134	103.9 %
	Distilled water	0	1	0.967	96.7 %
Hg^{2+}	Tap water	0	1	0.971	97.1 %
	Distilled water	0	1	0.945	94.5 %

4. Conclusions

This study systematically examined the etching processes and electrochemical properties of MoAlB-derived MBene. We demonstrated that various etchants, including APS, $CuCl_2$, H_2SO_4, and NaOH, significantly influence the etching efficiency and the structural integrity of the resultant MBenes. Alkali etching provided the highest purity MBene with an accordion-like structure, essential for electrochemical applications. High-temperature etching at 220°C facilitated complete Al removal but compromised the layered structure, highlighting the necessity of optimizing etching conditions to balance purity and structural integrity. Electrochemical studies revealed that OL-MBene-modified GCE exhibited excellent performance in detecting Cd^{2+}, Pb^{2+}, Cu^{2+}, and Hg^{2+} ions individually and simultaneously, with high sensitivity and selectivity. Pb^{2+} demonstrated the highest sensitivity due to its lowest

adsorption energy on the MBene surface. Competitive adsorption studies indicated that Pb^{2+} competes with Hg^{2+} for adsorption sites while having minimal impact on Cd^{2+} and Cu^{2+} adsorption. Moreover, the MBene@GCE sensing electrode demonstrated excellent reproducibility and stability, along with outstanding discrimination ability and selectivity, even when the concentration of interfering substances was ten times higher than that of the target ions. These findings underscore the potential of MBenes as effective materials for the next-generation electrochemical sensors, paving the way for further exploration and application in environmental monitoring and other fields.

CRediT authorship contribution statement

Shudan Wei: Visualization, Software, Project administration, Methodology, Investigation, Formal analysis, Data curation. **Girish Kale:** Writing – review & editing, Supervision. **Xiaojun Lai:** Writing – review & editing, Supervision.

Declaration of Competing Interest

The authors declare the following financial interests/personal relationships which may be considered as potential competing interests: Shudan Wei reports financial support was provided by China Scholarship Council. If there are other authors, they declare that they have no known competing financial interests or personal relationships that could have appeared to influence the work reported in this paper.

Acknowledgements

This work was supported by the China Scholarship Council - University of Leeds Scholarship (202006130007). We express our gratitude to the High-Performance Computing (ARC) platforms at the University of Leeds for facilitating the execution of CASTEP. Special thanks to Prof. Kevin Roberts and Dr. Caiyun Ma for their guidance in simulation.

Appendix A. Supporting information

Supplementary data associated with this article can be found in the online version at doi:10.1016/j.snb.2025.137258.

Data Availability

Data will be made available on request.

References

[1] J. Zhou, J. Palisaitis, J. Halim, M. Dahlqvist, Q.Z. Tao, I. Persson, L. Hultman, P.O. A. Persson, J. Rosen, Boridene: two-dimensional $Mo_{4/3}B_2$-X with ordered metal vacancies obtained by chemical exfoliation, Science 373 (2021) 801–805.
[2] K.N. Dinh, Q.H. Liang, C.F. Du, J. Zhao, A.L.Y. Tok, H. Mao, Q.Y. Yan, Nanostructured metallic transition metal carbides, nitrides, phosphides, and borides for energy storage and conversion, Nano Today 25 (2019) 99–121.
[3] S. Wei, G. Kale, X. Lai, Unlocking enhanced electrochemical performance of mbene-mob through controlled aluminum dissipation from moalb, Small N./a (2024) 2401573.
[4] A. Shukla, G. Sharma, S. Krishnamurty, Functionalized Mo_2BX_2 (X = H, OH, O) mbenes as a promising sensor, capturer and storage material for environmentally toxic gases: a case study of 1t and 2h phase, Appl. Surf. Sci. 615 (2023) 156299.
[5] Y. Pei, X. Zhang, Z. Hui, J. Zhou, X. Huang, G. Sun, W. Huang, $Ti_3C_2T_x$ Mxene for sensing applications: recent progress, design principles, and future perspectives, ACS Nano 15 (2021) 3996–4017.
[6] M.L. Desai, H. Basu, R.K. Singhal, S. Saha, S.K. Kailasa, Ultra-small two dimensional mxene nanosheets for selective and sensitive fluorescence detection of Ag^+ and Mn^{2+} ions, Colloids Surf. A: Physicochem. Eng. Asp. 565 (2019) 70–77.
[7] S. Pinilla, J. Coelho, K. Li, J. Liu, V. Nicolosi, Two-dimensional material inks, Nat. Rev. Mater. 7 (2022) 717–735.
[8] S. Wei, X. Lai, G.M. Kale, Exploring the potential of mbenes supercapacitors: fluorine-free synthesized $MoAl_{1-X}B$ with ultrahigh conductivity and open space, ACS Appl. Mater. Interfaces 15 (2023) 33560–33570.
[9] M.S. Javed, X. Zhang, T. Ahmad, M. Usman, S.S.A. Shah, A. Ahmad, I. Hussain, S. Majeed, M.R. Khawar, D. Choi, C. Xia, W. Al Zoubi, M.A. Assiri, A.M. Hassan, S. Ali, W. Han, Mxenes to mbenes: latest development and opportunities for energy storage devices, Mater. Today 74 (2024) 121–148.
[10] L.T. Alameda, P. Moradifar, Z.P. Metzger, N. Alem, R.E. Schaak, Topochemical deintercalation of al from moaib: stepwise etching pathway, layered intergrowth structures, and two-dimensional mbene, J. Am. Chem. Soc. 140 (2018) 8833–8840.
[11] M. Jakubczak, A. Szuplewska, A. Rozmyslowska-Wojciechowska, A. Rosenkranz, A. M. Jastrzebska, Novel 2D mbenes-synthesis, structure, and biotechnological potential, Adv. Funct. Mater. 31 (2021).
[12] K.J. Baumler, O.S. Adams, R.E. Schaak, One-step topochemical transformation of moalb into metastable Mo_2AlB_2 using a metal chloride salt reaction, Chem. Commun. 59 (2023) 4814–4817.
[13] J. Mou, S. Li, W. Zhang, W. Xu, S. Fan, G. Bei, Deintercalation of Al from moalb by molten salt etching to achieve a Mo_2AlB_2 compound and 2D MoB nanosheets, J. Adv. Ceram. 12 (2023) 943–953.
[14] M. Zhai, B. Fu, Y. Zhai, W. Wang, A. Maroney, A.A. Keller, H. Wang, J.-M. Chovelon, Simultaneous removal of pharmaceuticals and heavy metals from aqueous phase via adsorptive strategy: a critical review, Water Res. 236 (2023) 119924.
[15] X. Wang, L. Meng, M. Hu, L. Gao, B. Lian, The competitive and selective adsorption of heavy metals by struvite in the Pb(II)-Cd(II)-Zn(II) composite system and its environmental significance, Water Res. 250 (2024) 121087.
[16] X. Yu, Y. Wei, C. Liu, J. Ma, H. Liu, S. Wei, W. Deng, J. Xiang, S. Luo, Ultrafast and deep removal of arsenic in high-concentration wastewater: a superior bulk adsorbent of porous Fe_2O_3 nanocubes-impregnated graphene aerogel, Chemosphere 222 (2019) 258–266.
[17] Y. Wei, S. Wei, C. Liu, T. Chen, Y. Tang, J. Ma, K. Yin, S. Luo, Efficient removal of arsenic from groundwater using iron oxide nanoneedle array-decorated biochar fibers with high fe utilization and fast adsorption kinetics, Water Res. 167 (2019).
[18] J. Liu, J. Zhao, J. Du, S. Peng, J. Wu, W. Zhang, X. Yan, Z. Lin, Predicting the binding configuration and release potential of heavy metals on iron (Oxyhydr) Oxides: a machine learning study on exafs, J. Hazard. Mater. 468 (2024) 133797.
[19] Y. Zhou, Y. Tang, C. Liao, M. Su, K. Shih, Recent advances toward structural incorporation for stabilizing heavy metal contaminants: a critical review, J. Hazard. Mater. 448 (2023) 130977.
[20] L.A. Malik, A. Bashir, A. Qureashi, A.H. Pandith, Detection and removal of heavy metal ions: a review, Environ. Chem. Lett. 17 (2019) 1495–1521.
[21] V.N. Losev, O.V. Buyko, A.K. Trofimchuk, O.N. Zuy, Silica sequentially modified with polyhexamethylene guanidine and arsenazo i for preconcentration and icp–oes determination of metals in natural waters, Microchem. J. 123 (2015) 84–89.
[22] T. Gong, J. Liu, X. Liu, J. Liu, J. Xiang, Y. Wu, A sensitive and selective sensing platform based on cdte qds in the presence of L-cysteine for detection of silver, mercury and copper ions in water and various drinks, Food Chem. 213 (2016) 306–312.
[23] S. Tatay, P. Gaviña, E. Coronado, E. Palomares, Optical mercury sensing using a benzothiazolium hemicyanine dye, Org. Lett. 8 (2006) 3857–3860.
[24] S. Wang, P. Liao, L. Cen, H. Cheng, Q. Liu, Biochar promotes arsenopyrite weathering in simulated alkaline soils: electrochemical mechanism and environmental implications, Environ. Sci. Technol. 57 (2023) 8373–8384.
[25] Q. Tian, S. Chen, M. Shi, T. Gao, M. Zhang, C. Liao, X. Li, Q. Dong, C. Wang, Fluorine-functionalized mof modified gce for highly sensitive electrochemical detection of persistent pollutant perfluorooctanoic acid, Sens. Actuators B: Chem. 404 (2024) 135309.
[26] C. Jiang, S. Liu, T. Zhang, Q. Liu, P.J.J. Alvarez, W. Chen, Current methods and prospects for analysis and characterization of nanomaterials in the environment, Environ. Sci. Technol. 56 (2022) 7426–7447.
[27] S. Wu, X. Xing, W. Xiong, Z. Guo, H. Li, Oxidation state regulation of iron-based bimetallic nanoparticles for efficient and simultaneous electrochemical detection of Pb^{2+} and Cu^{2+}, Sens. Actuators B: Chem. 413 (2024) 135908.
[28] J.P. Perdew, K. Burke, M. Ernzerhof, Generalized gradient approximation made simple, Phys. Rev. Lett. 77 (1996) 3865–3868.
[29] Y. Zhou, H. Xiang, H. Zhang, F.-Z. Dai, Theoretical prediction on the stability, electronic structure, room and elevated temperature properties of a new mab phase Mo_2AlB_2, J. Mater. Sci. Technol. 35 (2019) 2926–2934.
[30] H.J. Monkhorst, J.D. Pack, Special points for brillouin-zone integrations, Phys. Rev. B 13 (1976) 5188–5192.
[31] M. Guo, C.B. Liu, Z.Z. Zhang, J. Zhou, Y.H. Tang, S.L. Luo, Flexible $Ti_3C_2T_x$@Al Electrodes with Ultrahigh Areal Capacitance: In Situ Regulation of Interlayer Conductivity and Spacing, Adv. Funct. Mater. 28 (2018).
[32] S. Muralikrishna, K. Sureshkumar, T.S. Varley, D.H. Nagaraju, T. Ramakrishnappa, In situ reduction and functionalization of graphene oxide with L-cysteine for simultaneous electrochemical determination of Cadmium(II), Lead(II), Copper(II), and Mercury(II) Ions, Anal. Methods 6 (2014) 8698–8705.
[33] X. Zhu, B. Liu, H. Hou, Z. Huang, K.M. Zeinu, L. Huang, X. Yuan, D. Guo, J. Hu, J. Yang, Alkaline intercalation of Ti_3C_2 Mxene for simultaneous electrochemical detection of Cd(II), Pb(II), Cu(II) and Hg(II), Electrochim. Acta 248 (2017) 46–57.
[34] R. Amunugama, M.T. Rodgers, Influence of substituents on cation−π interactions. 1. Absolute binding energies of alkali metal cation−toluene complexes determined by threshold collision-induced dissociation and theoretical studies, J. Phys. Chem. A 106 (2002) 5529–5539.
[35] A. Shah, A. Shah, Selective and simultaneous detection of Zn^{2+}, Cd^{2+}, Pb^{2+}, Cu^{2+}, Hg^{2+} and Sr^{2+} using surfactant modified electrochemical sensors, Electrochim. Acta 323 (2019) 134592.

Shudan Wei received her PhD degree from the School of Chemical and Process Engineering, University of Leeds, UK in 2024. Her research interests include electrocatalysis,

bioelectrochemistry, sensors, energy storage, wastewater treatment, functional materials, DFT simulation, and photocatalysis. She has published numerous highly cited papers in prestigious journals, including Chemical Engineering Journal, Small, Water Research, and Journal of Hazardous Materials.

Girish Kale joined the University of Leeds in 2006 and has dedicated his research career to the development of advanced functional materials for electrochemical sensor technology, focusing on applications in both ambient and high-temperature aggressive environments, such as combustion and metallurgical processes. His work encompasses both experimental research and theoretical analysis. He has authored 164 research articles in internationally peer-reviewed journals, including Sensors and Actuators B: Chemical, Journal of Materials Chemistry A, and presented more than 80 papers at international conferences.

Xiaojun Lai earned his PhD from the Department of Pure and Applied Chemistry at the University of Strathclyde, Glasgow, UK. He joined the School of Chemical and Process Engineering at the University of Leeds in 2004. His research focuses on environmental engineering, drug separation, crystallization engineering, and crystallography. He has published numerous papers in leading journals in these fields, such as 'Applied Catalysis B: Environmental' and 'Fuel'.